Structural Eng. / Earthquake Eng. Vol. 5. No. 2, 275s-283s. October 1988
Japan Society of Civil Engineers (Proc. of JSCE No. 398/I-10)

SOURCE INVERSION OF ACOUSTIC EMISSION WAVEFORM

*By Masayasu OHTSU**

Based on a generalized theory of acoustic emission which we previously proposed, an inverse procedure for the source characterization of AE is discussed. To determine the source kinematics (crack type and crack orientation), a moment tensor representation is introduced. It is clarified that the eigenvalue analysis of the moment tensor can afford essential information on the kinematics of crack movement. Then, an deconvolution analysis provides the kinetics of crack motion as a source-time function. To confirm the applicability of the source inversion procedure, numerical experiments are performed on the surface observation of AE. By employing simulated AE waveforms, source characteristics are inversely solved and determined. Results demonstrate a great promise of the proposed procedure for the source characterization of AE.

Keywords: *acoustic emission, source inversion, waveform analysis, moment tensor*

1. INTRODUCTION

Elastic waves during the energy release process in a solid are defined as acoustic emission (abbreviated as AE). Although AE characteristics in various materials have been studied extensively, our major concern is related with AE of concrete[1]. Theoretical studies of AE have been already performed and AE waveforms in concrete were simulated as elastic waves due to the displacement dislocations[2),3)].

Source mechanisms of AE are recently investigated by some groups[4),5)]. Force models equivalent to the displacement dislocation are mainly discussed[6)]. A dipole force model corresponding to a tensile crack and a double-couple force model corresponding to a shear crack are known. In contrast to these studies, we have proposed the characterization of AE sources, based on the displacement dislocation model. The theoretical treatment, later, is summarized as a generalized theory of AE[7),9)].

The source characterization of AE essentially belongs to an inverse problem. To identify AE sources, kinematics and kinetics must be determined. Conventionally, only information on the coordinates of AE source is obtained by the source location analysis[8)]. The aim of the present study is to develop a source inversion procedure of AE, based on the generalized theory. A proposed procedure is shown in Fig. 1. Taking into account the difference of P wave travel time, AE source is located. From the amplitude of P wave, a moment tensor is obtained. The classification of crack type and the determination of crack orientation can be performed by the eigenvalue analysis of the moment tensor. A deconvolution analysis provides information on source kinetics which is prescribed by a source-time function. To examine source kinematics and kinetics determined, a simulation analysis is available.

This source inversion is applied to the surface observation of AE waveforms in a thick plate, which is

* Member of JSCE, Dr. Eng., Associate Professor, Department of Civil and Environmental Engineering, Kumamoto University (Kurokami 2-39-1, Kumamoto 860)

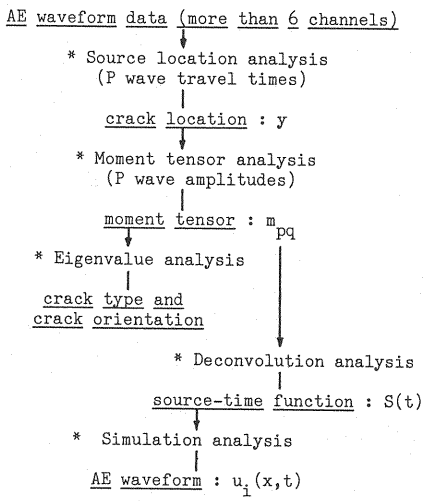

Fig. 1 A source inversion procedure proposed for AE waveforms.

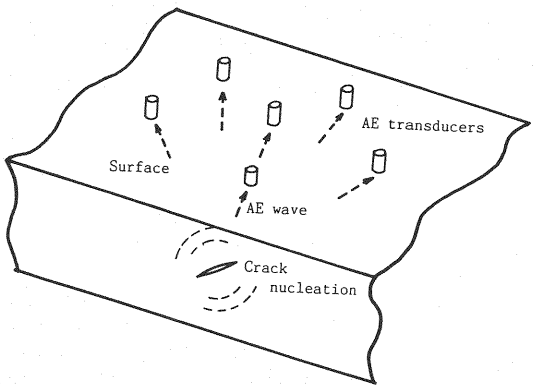

Fig. 2 A multi-channel AE observation of crack nucleation.

useful for pressure vessels and reinforced concrete slabs. AE sensors of a multi-channel system are arranged as shown in Fig. 2. AE waveforms due to crack nucleation are detected and analyzed by the proposed procedure.

2. THEORY OF ACOUSTIC EMISSION

Based on a generalized theory of AE[9], AE waveform $u_i(x, t)$ due to the displacement discontinuity $b_k(y, t)$ on crack surface F is represented by the integral representation,

$$u_i(x, t)=\int_F T_{ik}(x, y, t)* b_k(y, t)\, dS \quad \cdots\cdots (1)$$

Where $*$ denotes a convolution integral. T_{ik} is a traction associated with Green's function G_{ik} and is called Green's function of the second kind. By using elastic constant C_{pqjk} and an unit normal vector n_j to crack surface F, we have,

$$T_{ik}=C_{pqjk}G_{ip,q}(x, y, t)\, n_j \quad \cdots\cdots (2)$$

Here, $G_{ip,q}$ implies the spatial derivative of G_{ip} in respect to y_q.

Crack vector $b_k(y, t)$ corresponds to a Burgers vector in the dislocation theory. In the case of a small-scale dislocation, its time and spatial dependencies can be separated. Thus, eq. (1) becomes,

$$u_i(x, t)=T_{ik}(x, y, t)\, b l_k * S(t) \quad \cdots\cdots (3)$$

where $\int_F b_k(y, t)\, dS=b l_k S(t)$

Here, b represents the crack volume, vector l_k denotes the direction of crack movement. $S(t)$ denotes the time dependency of crack formation, which is called a source-time function.

For two cases shown in Fig. 3, the crack volume is easily estimated, as follow[10];

a) disk-shaped crack : $b=\pi a^2 h$

b) penny-shaped crack : $b=2\pi a^2 h/3$

where a is the radius of a crack and h is the crack opening displacement.

In the case that appropriate function $S(t)$ and crack volume b are known, a simulation analysis of AE waveform can be performed. A crack model embedded in a half space is considered as shown in Fig. 4. A tensile penny-shaped crack is located at 3 cm depth. Simulated AE waveforms are detected at $x_1=3$ cm for two cases of inclined angles with horizontal angle $\phi=0°$. Results computed by eq. (3) are shown in Fig. 5. Green's functions of the second kind in a half space were computed by using the programs previously

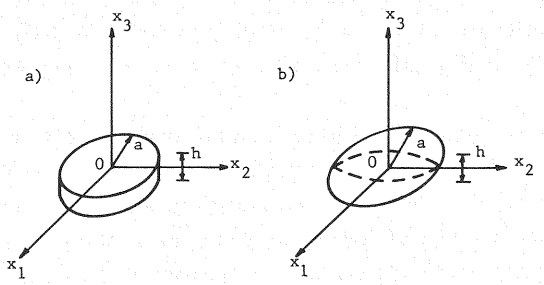

Fig. 3 a) A disk-shaped crack model.
b) A penny-shaped crack model.

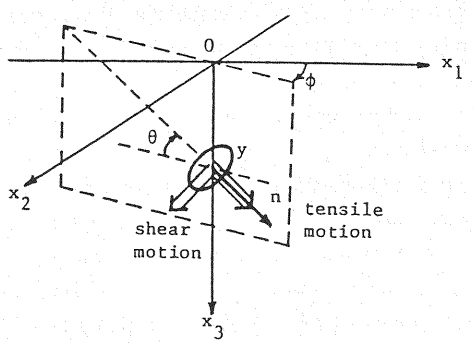

Fig. 4 An inclined crack model embedded at location y in a half space.

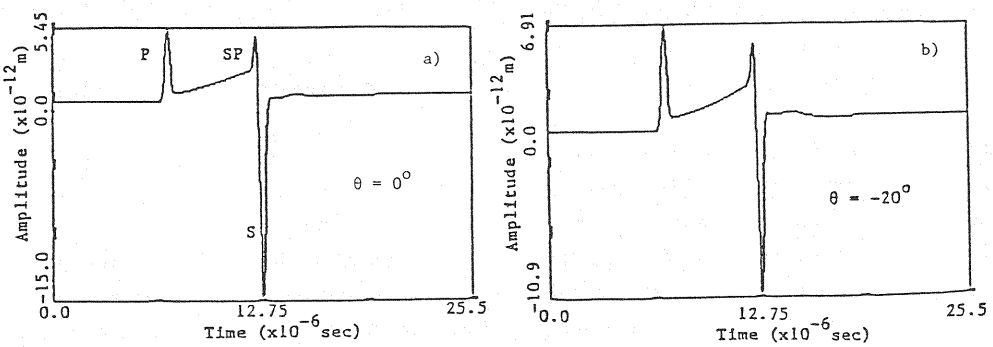

Fig. 5 Simulated AE waveforms due to tensile penny-shaped cracks of a) the case $\theta=0°$ and b) $\theta=-20°$.

published[9]. P wave velocity was assumed to be 6 400 m/s and Poisson's ratio ν was 0.3. Crack dimensions of a and h were 0.025 mm and 0.005 mm, respectively. A source-time function employed is expressed,

$$S(t)=t/T_r-2\sin(2\pi t/T_r)/(3\pi)+\sin(4\pi t/T_r)/(12\pi), \quad (0<t<T_r) \cdots\cdots (4)$$

where T_r is the rise time. In two graphs of Fig. 5, rise time T_r was 1 μs

Since AE waveforms are computed in a half space, SP wave which corresponds to P wave generated by the surface reflection of S wave is observed together with direct P wave and S wave. Neither reflections at other boundaries than the surface nor the resonance vibration of AE sensor is taken into account. It is confirmed, however, that the first portion of detected AE waveforms agree well with these simulated waveforms during the disbonding process of stainless steel overlay from base metal[11].

3. MOMENT TENSOR REPRESENTATION

The moment tensor representation is derived from eq. (3), substituting eq. (2),

$$u_i(x, t)=G_{ip,q}(x, y, t)\, m_{pq} * S(t) \cdots\cdots (5)$$

where m_{pq} is called a moment tensor and equal to $C_{pqjk}n_j l_k$. In the case of isotropic material, m_{pq} is expressed, as follows;

$$m_{pq}=b[\lambda l_j n_j \delta_{pq}+\mu(n_p l_q+n_q l_p)] \cdots\cdots (6)$$

Here, λ and μ are Lamé constants. Since elastic constant C_{pqjk} is a fourth-rank tensor and $n_j l_k$ constitutes a tensor product, moment tensor m_{pq} is obviously the second-rank tensor. Although dipole forces and force couples are known as the equivalent force model[5),6)], this concept is unnecessary in explaining the moment tensor representation. Components of a tensor can not be referred to as forces (vectors).

The case of a tensile crack with the direction vector of (1, 0, 0) and unit normal of (1, 0, 0) is shown in Fig. 6 a). The corresponding components of the moment tensor are obtained from eq. (6) and are

indicated in Fig. 6 c). To emphasize the nature of the second-rank tensor, the infinitesimal cubic element is not located at the origin of the coordinates. In this case, only normal components are observed. The case of a shear crack with the direction vector of (0, 1, 0) and normal vector of (1, 0, 0) is shown in Fig. 6 b). Tensor components obtained from eq. (6) are indicated in Fig. 6 d). Only off-diagonal are present on a cubic element.

Principal components of the second-rank tensor can be obtained from the eigenvalue analysis. For an inclined tensile crack of the direction vector ($\cos\theta$, 0, $\sin\theta$) and a shear crack of ($\sin\theta$, 0, $-\cos\theta$) on a crack surface with normal vector ($\cos\theta$, 0, $\sin\theta$), results of the eigenvalue analysis are presented in Fig. 7. Graphs show the first two eigenvectors with the magnitude of eigenvalues on the x_1-x_3 plane. The radiation patterns of P wave[12] are also plotted in the same figure. As can be seen, eigenvectors with the magnitude of eigenvalues constitute the principal axes of the radiation pattern.

Three eigenvalues can be calculated from eq. (6), as follow[13];

the maximum eigenvalue : $\mu b\,(l_k n_k/(1-2\nu)+1)$,

the medium eigenvalue : $2\mu b\nu l_k n_k/(1-2\nu)$,

and the minimum eigenvalue : $\mu b\,(l_k n_k/(1-2\nu)-1)$

Here, a relationship $\lambda=2\mu\nu/(1-2\nu)$ is employed. Three eigenvectors corresponding to these eigenvalues are also determined,

the eigenvector for the maximum value : l_k+n_k,

the eigenvector for the medium value : $e_{ijk}l_i n_j$,

and the eigenvector for the minimum value : l_k-n_k

In the case of a pure shear crack, the direction of crack movement, l_k, is vertical to normal vector n_k. It means that $l_k n_k$ is equal to zero. Three eigenvalues become μb, 0, and $-\mu b$. Two eigenvalues are of equal magnitude and opposite direction. For a pure tensile crack, the direction of crack movement is identical to the normal vector, that is, $l_k n_k=1$. Three eigenvalues are $2\mu b\,(1-\nu)/(1-2\nu)$, $2\mu b\nu/(1-2\nu)$, and $2\mu b\nu/(1-2\nu)$. These components can be decomposed into deviatoric components and hydrostatic mean components. In seismology, deviatoric components are known as the compensated linear vector dipole (CLVD)[14]. Three deviatoric components are $4/3\,\mu b$, $-2/3\,\mu b$, and $-2/3\,\mu b$. A mean component corresponds $2\mu b\,(1+\nu)/3\,(1-2\nu)$.

In a practical situation, AE sources may consist of a tensile motion and a shear motion. Thus, the characteristics of the moment tensor leads to a technique to decompose eigenvalues into three components. Setting the ratio of shear component as $(X, 0, -X)$, that of CLVD component as $(Y, -0.5\,Y, -0.5\,Y)$, and mean component as Z, the ratios of eigenvalues are uniquely decomposed,

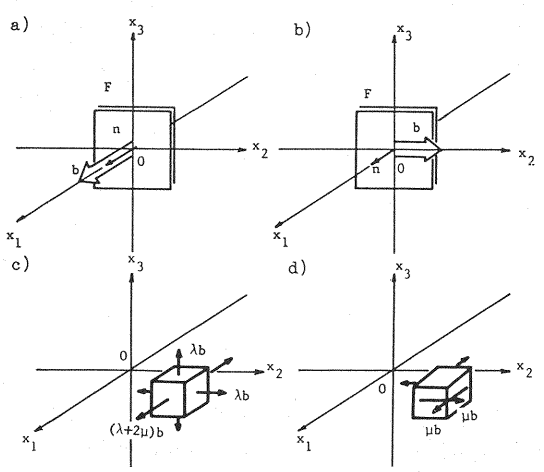

Fig. 6 a) A dislocation model for a tensile crack and b) that for a shear crack on the crack surface. c) Normal components for a tensile crack and d) corresponding off-diagonal components for a shear crack.

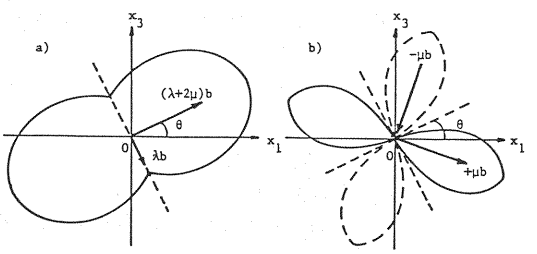

Fig. 7 a) The radiation pattern of P wave due to a tensile crack and eigenvectors with the magnitude of eigenvalues. b) The radiation pattern of P wave due to a shear crack and eigenvectors with the magnitude of eigenvalues.

$$1.0=X+Y+Z,$$

The medium eigenvalue/the maximum eigenvalue $=0-0.5\,Y+Z$,

The minimum eigenvalue/the maximum eigenvalue $=-X-0.5\,Y+Z$.

These ratios are illustrated in Fig. 8. Note that components of both shear model and CLVD model are deviatoric.

Since the eigenvector for the maximum eigenvalue directs the direction of a tensile motion, crack orientation of tensile type is determined from the direction of the first eigenvector. For shear cracks, either the direction of crack motion l_k or unit normal n_k is determined from the sum of the first and the third eigenvectors.

4. DETERMINATION OF MOMENT TENSOR COMPONENTS

To determine moment tensor components from AE waveform, the contribution of P wave is selected from eq. (5) in the case of infinite space. The convolution integral, $G_{ip,q} * S(t)$ becomes[15],

$$G_{ip,q}(x,\ y,\ t)*S(t)=[15\ r_i r_p r_q-3\ (\delta_{ip}r_q+\delta_{iq}r_p+\delta_{pq}r_i)]/(4\ \pi\rho R^2)\int_{1/v_p}^{1/v_s}\lambda S\ (t-\lambda R)\,d\lambda$$
$$+[6\ r_i r_p r_q-(\delta_{ip}r_q+\delta_{iq}r_p+\delta_{pq}r_i)]/(4\ \pi\rho R^2 v_p^2)\ S\ (t-R/v_p)+[-6\ r_i r_p r_q+2\ \delta_{ip}r_q+\delta_{iq}r_p+\delta_{pq}r_i]/$$
$$(4\ \pi\rho r^2 v_S^2)\ S\ (t-R/v_S)+[r_i r_p r_q]/(4\ \pi\rho R v_p^3)\,dS\ (t-R/v_p)/dt+[\delta_{ip}r_q-r_i r_p r_q]/$$
$$(4\ \pi\rho R v_S^3)\,dS\ (t-R/v_S)/dt \quad \cdots\cdots (7)$$

Where R is the distance from source location y to observation point x and r_i is its direction cosine. ρ is the mass density. v_p and v_s are P wave velocity and S wave velocity of the material, respectively. The dominant contribution from P wave is represented in the second term and the fourth term in eq. (7). The second term decreases with the order of $1/R^2$, while the fourth term decreases only with the order of $1/R$. The fourth term is known as the far-field term in seismology[16]. Since AE waves are observed in the near field, it seems that both terms have to be taken into account.

Considering the amplitude ratio of the second term to the fourth term, we have,

the second term : the fourth term $=1/R^2 v_p^2 S(t) : 1/R v_p^3 dS(t)/dt$

Since v_p is larger than R in the case of AE waves, it seems that the second term is bigger than the fourth. However, $dS(t)/dt$ has the order of $1/T_r$ from eq. (4) and T_r is usually a few microseconds. Eventually, the fourth term in eq. (7) has the dominant effect on the first motion.

Substituting the fourth term in eq. (7) into eq. (5) and setting the direction vector of the sensor vibration as e_i, detecting amplitude A at a sensor location becomes,

$$A=u_i(x)\,e_i=C\ (r_i e_i)/R\ (r_1 r_1 m_{11}+2\ r_1 r_2 m_{12}+2\ r_1 r_3 m_{13}+r_2 r_2 m_{22}+2\ r_2 r_3 m_{23}+r_3 r_3 m_{33}) \quad \cdots\cdots (8)$$

where $C=1/(4\ \pi\rho v_p^3)\ dS/dt$. Because only the amplitude of the first motion (P wave) is taken into account, the time dependency is omitted.

When elastic waves due to one AE event are detected at several locations, the amplitudes of the first motions correspond to the left-hand-side of eq. (8) in the case of infinite space. For other cases, the reflection calibration must be carried out. The application to AE waveforms detected by embedded sensors was already reported in the hydrofracturing process[17].

Setting the angle between the direction of sensor vibration and the direction from the source to the sensor as θ, reflection coefficient R_e becomes[16],

$$R_e=2\,k^2\,(k^2-2\sin^2\theta)/[(k^2-2\sin^2\theta)^2+4\sin^2\theta\cos\theta\sqrt{k^2-\sin^2\theta}]$$

where $k=v_p/v_s$ and $\cos\theta$ correspons to the direction cosine $r_i e_i$.

The effect of the reflection coefficient was studied by numerical experiments. Simulated AE waveforms due to tensile cracks in a half space were computed in the same manner as those in Fig. 5. Then, AE waveforms in an infinite space were computed, based on eq. (7) and were calibrated by the reflection coefficient. Comparisons are shown in Fig. 9. Resonable agreement is observed. It confirms the

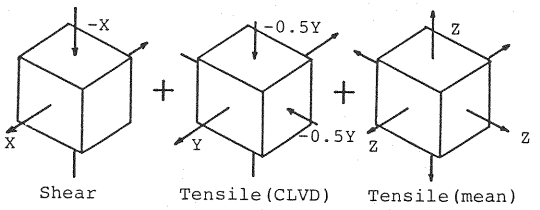

Fig. 8 Decomposition of eigenvalues into shear, CLVD, and mean components.

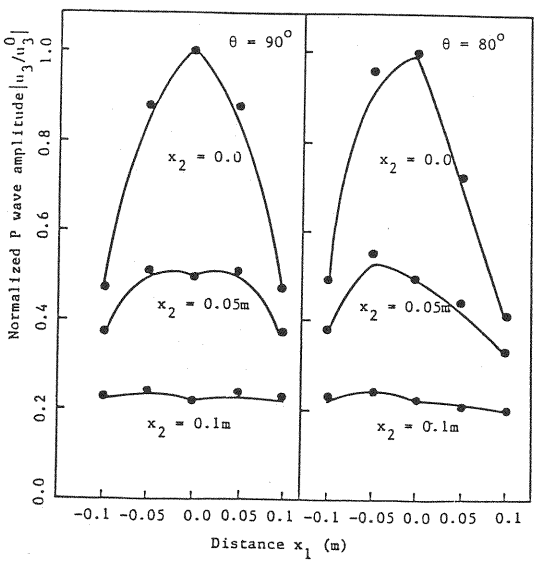

Fig. 9 Solid curves show the first motions in a half space due to tensile cracks. Solid circles indicate those in an infinite space, which are calibrated by the reflection coefficient.

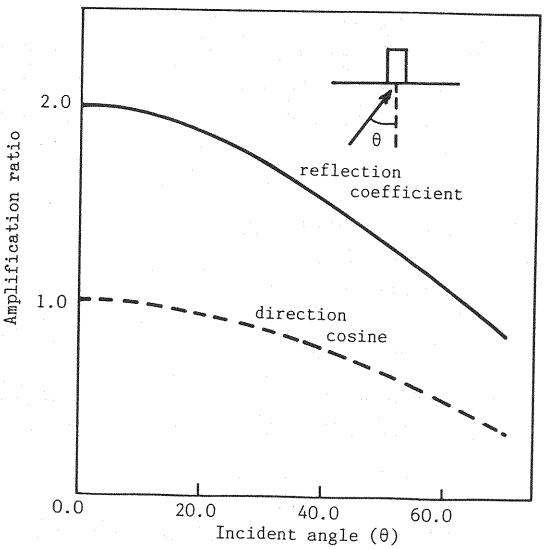

Fig. 10 Comparison between the reflection coefficient and the direction cosine for various incident angles.

applicability of the reflection calibration.

Furthermore, values of the reflection coefficient were compared with those of the direction cosine for various incident angles. Results are shown in Fig. 10. The values of reflection coefficient is almost the double of those of the direction cosine, for the cases of the incident angle less than 40°. It implies that the reflection calibration may be performed by the direction cosine except for oblique incidence.

The source location analysis provides information on distance R and the direction cosines γ_i. Thus, a set of linear algebraic equations is obtained with unknown values of m_{pq}, after the reflection calibration in eq. (8). Since relative amplitudes are interested, the minimum requirement for the measurement is the equivalent sensitivity of each detecting channel. As a result, care for the sensor selection become inconsequential in this procedure.

5. SOURCE INVERSION AND DISCUSSION

To check the feasibility of the source inversion procedure, numerical experiments for pure tensile and shear cracks were carried out. Considering crack models as shown in Fig. 4 at 5 cm depth, simulated AE waveforms were detected at nine sensor locations shown in Fig. 11. Prior to the inversion, components of moment tensors in four cases indicated in Table 1 were calculated from eq. (6). Results are shown in the table as "exact", which are normalized by the maximum value.

In the similar manner to waveforms in Fig. 5, the simulation analysis due to tensile and shear cracks in the cases of Table 1 were performed. Reading travel time differences and relative amplitudes as seen in Fig. 12, the source inversion procedure was applied to these simulated AE waveforms in a half space. By employing the source location algorithm[8], locations of AE sources were obtained with enough accuracy. Then, moment tensor components were determined from eq. (8), taking the reflection coefficient into consideration. Results of tensor components are indicated in Table 1 as "determined". Although only the

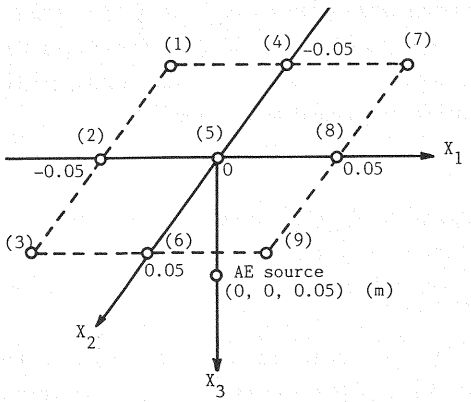

Fig. 11 AE sensor locations assumed in numerical experiments.

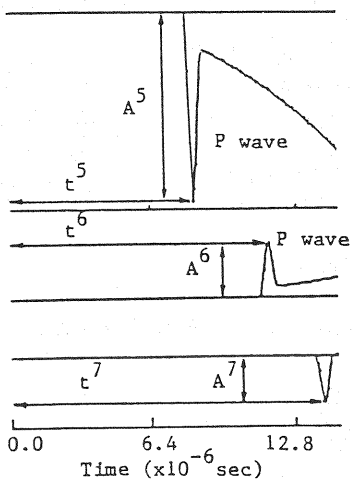

Fig. 12 Amplitudes of P wave and travel time differences at sensor locations (5), (6), and (7).

Table 1 Moment tensor components obtained for crack models assumed and results of the source inversion.

	exact			determined		
tensile	1.000	0.149	0.100	1.000	0.152	0.101
$\theta = 10^\circ$		0.492	0.027		0.465	0.027
$\phi = 15^\circ$	Sym.		0.471	Sym.		0.451
tensile	1.000	0.371	0.191	1.000	0.396	0.199
$\theta = 20^\circ$		1.000	0.191		1.000	0.199
$\phi = 45^\circ$	Sym.		0.728	Sym.		0.732
shear	-0.352	-0.094	1.000	-0.384	-0.095	1.000
$\theta = 10^\circ$		-0.025	0.268		-0.045	0.268
$\phi = 15^\circ$	Sym.		0.377	Sym.		0.393
shear	-0.500	-0.500	0.843	-0.541	-0.521	0.856
$\theta = 20^\circ$		-0.500	0.843		-0.541	0.856
$\phi = 45^\circ$	Sym.		1.000	Sym.		1.000

Table 2 Results of the eigenvalue analysis.

eigenvalue	components	direction
1.000	shear= 0.8%	tensile
0.409	clvd =38.9%	$\theta = 9.8^\circ$
0.401	mean =60.4%	$\phi = 14.8^\circ$
1.000	shear= 1.7%	tensile
0.419	clvd =37.6%	$\theta = 20.1^\circ$
0.403	mean =60.7%	$\phi = 45.0^\circ$
1.000	shear=97.4%	shear
0.018	clvd = 1.5%	$\theta = 10.9^\circ$
-0.986	mean = 1.1%	$\phi = 14.9^\circ$
1.000	shear=97.4%	shear
0.012	clvd = 0.9%	$\theta = 20.0^\circ$
-0.962	mean = 1.7%	$\phi = 45.0^\circ$

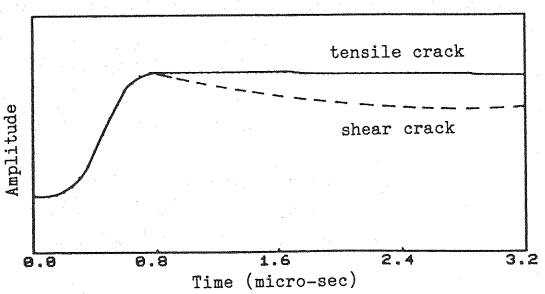

Fig. 13 Source-time functions obtained by the deconvolution analysis.

fourth term of eq. (7) is taken into account, reasonable agreement between exact values and those determined is observed.

The eigenvalue analysis corresponding to four cases in Table 1 was carried out. Results are shown in Table 2. Although slight discrepancies are observed in tensor components, the decomposition provides the good inversion of sources. The discrepancies between the assumed models and the determined models are 0.8 % and 1.7 % for tensile cracks, and those are 2.6 % for shear cracks. It shows the usefulness of the eigenvalue decomposition for determining crack types.

Directions of crack motions are determined from the eigenvectors. Results are indicated in the same table. It is observed that the directions of crack motions are determined within 1 % error.

As discussed in Fig. 1, the deconvolution analysis can be performed after determining moment tensor components. Observed waveforms correspond to the left-hand-side in eq. (5). The spatial derivatives of Green's functions in a half space $G_{ip,q}$ and moment tensor components m_{pq} are known. Substituting AE

waveforms into $u_i(t)$, eq. (5) becomes an integral equation with unknown function $S(t)$. Analyzed results of the deconvolution analysis are shown in Fig. 13. For the cases of tensile and shear cracks with $\phi = 45^\circ$ were analyzed. For a shear crack, a slight discrepancy is observed after the rising portion. However, since the rise time assumed was 1 μs, reasonable agreement is obtained.

6. CONCLUSION

A source inversion procedure for determining crack types and crack orientations (source kinematics) is investigated in acoustic emission (AE). Results are summarized, as follow;

(1) On the basis of a generalized theory of AE, fundamental characteristics of the moment tensor are clarified.

(2) Results lead to the unique decomposition of eigenvalues into shear component, compensated linear vector dipole component, and mean component. Based on ratios of these components, AE sources are classified into either a shear crack or a tensile crack.

(3) Eigenvectors of the moment tensor provide information on crack orientation. It is also clarified that these vectors with the magnitude of eigenvalues correspond to the principal axes of the radiation pattern of P wave.

(4) The inversion procedure is applied to the surface observation of AE waves. Results confirm a great promise for classifying AE sources and for determining crack orientations. The proposed technique is simple enough to be readily incorporated into computer-based AE waveform analyzers.

REFERENCES

1) Niwa, Y., Kobayashi, S. and Ohtsu, M. : Studies of Acoustic Emission in Concrete structures, Proc. JSCE, No. 261, pp. 101~112, 1977 (in Japanese).
2) Niwa, S., Kobayashi, S. and Ohtsu, M. : Source Mechanisms of Acoustic Emission, Proc. JSCE, No. 314, pp. 125~136, 1981 (in Japanese).
3) Ohtsu, M. : Source Mechanism and Waveform Analysis of Acoustic Emission in Concrete, J. Acoustic Emission, Vol. 1, No. 2, pp. 103~112, 1982.
4) Hsu, N. N. and Hardy, S. C. : Experiments in Acoustic Emission Waveform Analysis for Characterization of AE Sources, Sensors and Structures, *Elastic Waves and Non-destructive Testing of Materials*, AMD-Vol. 29, pp. 85~106, 1978.
5) Wadley, H. N. G. and Scruby, C. B. : Acoustic Emission Source Characterization, *Advances in Acoustic Emission*, eds. Dunegan, H. L. and Hartman, W. F., Dunhart Publishers, Knoxville, pp. 125~153, 1981.
6) Ohira, T., Kishi, T. and Ohisa, N. : Acoustic Emission Source Characterization, Japanese Committee on Acoustic Emission, No. 006-19, JSNDI, pp. 1~24, 1982.
7) Ohtsu, M. and Ono, K. : The Generalized Theory and Source Representations of Acoustic Emission, J. Acoustic Emission, Vol. 5, No. 4, pp. 124~133, 1986.
8) Niwa, Y., Kobayashi, S. and Ohtsu, M. : Studies of Source Location by Acoustic Emission, Proc. JSCE, No. 276, pp. 135~147, 1978 (in Japanese).
9) Ohtsu, M. and Ono, K. : A Generalized Theory of Acoustic Emission and Green's Functions in A Half Space, J. Acoustic Emission, Vol. 3, No. 1, pp. 27~40, 1984.
10) Ohtsu, M., Yuyama, S. and Imanaka, T. : Theoretical Treatment of Acoustic Emission Sources in Microfracturing due to Disbonding, J. Acoust. Soc. Am., Vol. 82, No. 2, pp. 506~512, 1987.
11) Ohtsu, M. : Mathematical Theory of Acoustic Emission and Moment Tensor Solution, J. Soc. Mat. Sci., Japan (Zairyo), Vol. 36, No. 408, pp. 1025~1031, 1987 (in Japanese).
12) Ohtsu, M. : Radiation Pattern of Acoustic Emission, J. Soc. Mat. Sci., Japan (Zairyo), Vol. 32, No. 356, pp. 577~583, 1983 (in Japanese); Translated as DRIC-T-7599, Defence Research Information Center, Procurement Executive Ministry of Defence (1985).
13) Ohtsu, M. : Determination of Crack Orientation by Acoustic Emission, Materials Evaluation, Vol. 45, No. 9, pp. 1070~1075, 1987.
14) Knopoff, L. and Randall, M. J. : The Compensated Linear-Vector Dipole : A Possible Mechanism for Deep Earthquakes, J. Geophys. Res., Vol. 75, No. 26, pp. 4957~4963, 1970.
15) Eringen, A. C. and Suhubi, E. S. : *Elastodynamics, Volume II Linear Theory*, Academic Press, 1975.

16) Aki, K. and Richards, P. G. : ***Quantitative Seismology Theory and Methods***, W. H. Freeman and Company, San Francisco, 1980.
17) Ohtsu, M., Ishida, T. and Sasaki, S. : Source Inversion Analysis of Acoustic Emission due to Hydrofracturing, Proc. 3rd Domestic Conference on Subsurface AE, JSNDI and MMIJ, pp. 20～26, 1988.

(Received January 9 1988)